Mitigation of Lower Order Harmonics in a Grid Connected Single Phase PV Inverter

Abhijit Kulkarni, *Student Member, IEEE,* and Vinod John, *Senior Member, IEEE*

***Abstract*—In this paper, a simple single phase grid connected photovoltaic (PV) inverter topology consisting of a boost section, a low voltage single phase inverter with an inductive filter and a step-up transformer interfacing the grid is considered. Ideally, this topology will not inject any lower order harmonics into the grid due to high frequency PWM operation. However the non-ideal factors in the system such as core saturation induced distorted magnetizing current of the transformer and the dead-time of the inverter, etc. contribute to a significant amount of lower order harmonics in the grid current. A novel design of inverter current control that mitigates lower order harmonics is presented in this paper. An adaptive harmonic compensation technique and its design is proposed for the lower order harmonic compensation. In addition, a Proportional-Resonant-Integral (PRI) controller and its design is also proposed. This controller eliminates the dc component in the control system, which introduce even harmonics in the grid current in the topology considered. The dynamics of the system due to the interaction between the PRI controller and adaptive compensation scheme is also analysed. The complete design has been validated with experimental results and good agreement with theoretical analysis of the overall system is observed.**

***Index Terms*—Solar Energy, Harmonic distortion, Adaptive filters, Inverters**

I. Introduction

Renewable sources of energy such as solar, wind, geothermal have gained popularity due to the depletion of conventional energy sources. Hence, many Distributed Generation (DG) systems making use of the renewable energy sources are being designed and connected to grid. In this paper, one such DG system with solar energy as the source is considered.

The topology of the solar inverter system is simple. It consists of the following three power circuit stages:

- A boost converter stage to perform maximum power point tracking (MPPT),
- A low voltage single phase H-bridge inverter,
- An inductive filter and a step-up transformer for interfacing with the grid.

Fig. 1 shows the power circuit topology considered. This topology has been chosen due to the following advantages: The switches are all rated for low voltage which reduces the cost and lesser component count in the system improves the overall reliability. This topology will be a good choice for low rated PV inverters of rating less than a kilowatt. The disadvantage would be the relatively larger size of the interface transformer compared to topologies with high frequency link transformer [1].

The system shown in Fig. 1 will not have any lower order harmonics in the ideal case. However the following factors result in lower order harmonics in the system: The distorted magnetizing current drawn by the transformer due to the non-linearity in the B-H curve of the transformer core, the dead-time introduced between switching of devices of the same leg [2]–[6], on-state voltage drops on the switches and the distortion in the grid voltage itself.

There can be a dc injection into the transformer primary due to a number of factors. These can be the varying power reference from a fast MPPT block from which the ac current reference is generated, the offsets in the sensors and A/D conversion block in the digital controller. This dc injection would result in even harmonics being drawn from the grid, again contributing to a lower power quality.

It is important to attenuate these harmonics in order for the PV inverter to meet standards such as IEEE 519-1992 [7] and IEEE 1547-2003 [8]. Hence, this work concentrates on the design of the inverter current control to achieve a good attenuation of the lower order harmonics. It must be noted that attenuating the lower order harmonics using a larger output filter inductance is not a good option as it increases losses in the system along with a larger fundamental voltage drop and with a higher cost. The boost stage and the MPPT scheme are not discussed in this paper as a number of methods are available in literature to achieve a very good MPPT [9]–[13].

There has been considerable research work done in the area of harmonic elimination using specialized control. In [15]–[22], multi-resonant controller based methods are used for selective harmonic elimination. The advantage of these methods is the simplicity in implementation of the resonant blocks. However, discretization and variations in grid frequency affect the performance of these controllers and making them frequency adaptive increases overall complexity [21], [22]. Also, as mentioned in [19], [21], [22], the phase margin of the system becomes small with multi-resonant controllers and additional compensation is required for acceptable operation. References [23]–[25] consider the use of repetitive controller based harmonic elimination which involves complicated analysis and design. As mentioned in [26] the performance of the repetitive controller is very sensitive to frequency variations and needs structural change for better performance, which might affect the stability.

In [27]–[31], adaptive filter based controllers are considered for harmonic compensation. Reference [27] uses an adaptive filter to estimate a harmonic and then adds it to the main

Manuscript received August 28, 2012. Accepted for publication December 28, 2012.

The authors are with the Department of Electrical Engineering, Indian Institute of Science, Bangalore 560012, India (e-mail: abhijitk@ee.iisc.ernet.in; vjohn@ee.iisc.ernet.in).

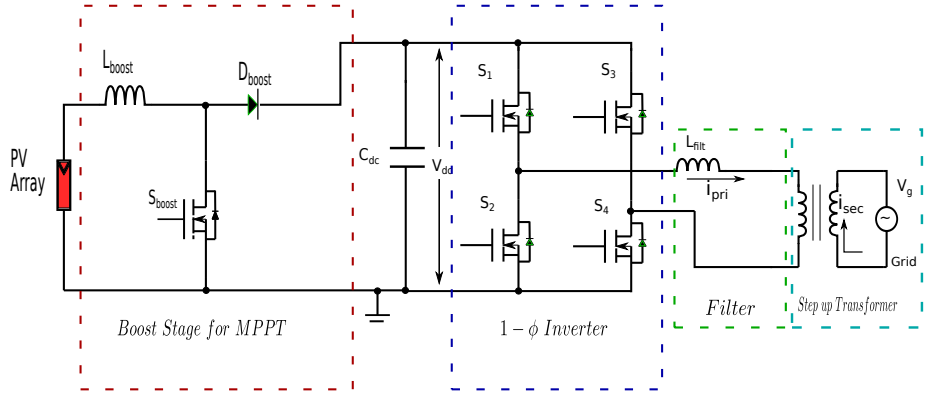

Fig. 1. Power circuit topology of the $1-\phi$ PV system for a low voltage inverter with $40V$ dc bus connected to $230V$ grid using a step up transformer.

current reference. Then multi-resonant block is used to ensure zero steady state error for that particular harmonic reference. Thus [27] uses both adaptive and multi-resonant scheme increasing overall complexity. Similar approaches are found in [28], [29] which add the harmonic current reference estimated using adaptive filters and use hysteresis controller for the reference tracking. Usage of hysteresis controller makes it difficult to quantify the effectiveness of this scheme. Reference [30] uses adaptive filter based method for dead-time compensation in rotating reference frame, which is not suitable in single phase systems. The method proposed in [31] requires an inverse transfer function of the system and is proposed for grid connected topology assuming the connection to be purely inductive.

The advantage of adaptive filter based method is the inherent frequency adaptability which would result in same amount of harmonic compensation even when there are shifts in grid frequency. The implementation of adaptive filters is simple. Thus in this paper, an adaptive filter based method is proposed. This method estimates a particular harmonic in the grid current using a Least-Mean-Square (LMS) adaptive filter and generates a harmonic voltage reference using a proportional controller. This voltage reference is added with appropriate polarity to the fundamental voltage reference to attenuate that particular harmonic. This paper includes an analysis to design the value of the gain in the proportional controller to achieve an adequate level of harmonic compensation. The effect of this scheme on overall system dynamics is also analysed. This method is simple for implementation and hence it can be implemented in a low-end digital controller.

Presence of dc in the inverter terminal voltage results in a dc current flow into the transformer primary. This dc current results in drawing of even harmonics from grid. If the main controller used is a PR controller, any dc offset in control loop will propagate through the system and the inverter terminal voltage will have a non-zero average value. Thus in this paper, a modification to conventional PR controller scheme is proposed. An integral block is used along with the PR controller to ensure that there is no dc in the output current of the inverter. This would automatically eliminate the even harmonics. This scheme is termed as PRI control and the design of the PRI controller parameters is provided. The complete scheme is verified experimentally and the results show a good correspondence with the analysis. Experimental results also show that the transient behaviour of the system is in agreement with the theoretical prediction.

The organization of the paper is as follows: Section II discusses the sources of lower order harmonics in the system and the design of fundamental current control using a PRI controller. In Section III, the concept of adaptive harmonic compensation is explained along with its design. The stability considerations of the system with the harmonic compensation block are discussed. In Section IV, parameters of the real system and experimental results are provided. Conclusions are given in Section V.

II. Origin of Lower Order Harmonics and Fundamental Current Control

This section discusses the origin of the lower order harmonics in the system under consideration. The sources of these harmonics are not modelled as the method proposed to attenuate them works independent of the harmonic source. The fundamental current control using the proposed PRI controller is also explained.

A. Origin of lower order harmonics

1) Odd harmonics: The dominant causes for the lower order odd harmonics are the distorted magnetizing current drawn by the transformer, the inverter dead-time and the semiconductor device voltage drops. Other factors are the distortion in the grid voltage itself and the voltage ripple in the dc bus.

The magnetizing current drawn by the transformer contains lower order harmonics due to the non linear characteristics of the B-H curve of the core. The exact amplitude of the harmonics drawn can be obtained theoretically if the B-H curve of the transformer is known [32]. The phase angle of the harmonics due to the magnetizing current will depend on the power factor of operation of the system. As the operation will be at unity power factor (UPF), the current injected to the grid will be in phase with the grid voltage. However, the magnetizing current lags the grid voltage by 90°. Hence, the harmonic currents will have a phase displacement of either $+90^o$ or -90° depending on harmonic order.

The dead-time effect introduces lower order harmonics which are proportional to the dead-time, switching frequency and the dc bus voltage. The dead-time effect for each leg of the inverter can be modelled as a square wave error voltage out of phase with the current at the pole of the leg [2]–[6]. The device drops also will cause a similar effect but the resulting amount of distortion is smaller compared that due to the dead-time. Thus for a single phase inverter topology considered, net error voltage is the voltage between the poles and is out of phase with the primary current of the transformer. The harmonic voltage amplitude for a hth harmonic can be expressed as

$$V_{error} = \frac{4}{h\pi}\frac{2V_{dc}t_d}{T_s} \tag{1}$$

Where t_d is the dead-time, T_s is the device switching frequency and V_{dc} is the dc bus voltage. Using the values of the filter inductance, transformer leakage inductance and the net series resistance, the harmonic current magnitudes can be evaluated. Again, it must be noted that the phase angle of the harmonic currents in this case will be 180° for UPF operation.

Thus it can be observed that the net harmonic content will have some phase angle with respect to the fundamental current depending on the relative magnitudes of the distortions due to the magnetizing current and the dead-time.

2) Even Harmonics: The topology under consideration is very sensitive to the presence of dc offset in the inverter terminal voltage. The dc offset can enter from a number of factors such as varying power reference given by a fast MPPT block, the offsets in the A/D converter and the sensors. To understand how a fast MPPT introduces a dc offset consider Fig. 2 and Fig. 3. In Fig. 2, d_{boost} is the duty ratio command given to the boost converter switch, V_{pv}, i_{pv} are the panel voltage and current respectively, P_{pv} is the panel output power, V_g is the rms value of the grid voltage, $\sin\theta$ is the in-phase unit vector for the grid voltage and i^* is the reference to the current control loop from MPPT block. As the power reference keeps

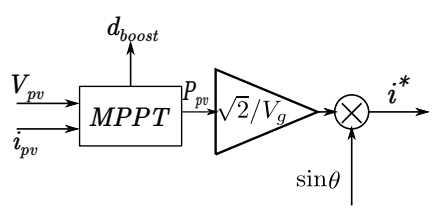

Fig. 2. Generation of inverter ac current reference from MPPT block.

on changing due to fast MPPT action, the current reference may have a non-zero average value, which is illustrated in Fig. 3 for a step change in power reference which repeats.

Assume that a certain amount of dc exists in the current control loop. This will result in applying a voltage with a dc offset across the L-filter and the transformer primary. The net average current flowing in the filter and the transformer primary loop will be determined by the net resistance present in the loop. This average current will cause a dc shift in the B-H curve of the transformer [33]–[35]. This shift would mean an asymmetric non linear saturation characteristic which causes the transformer magnetizing current to lose its half-wave symmetry. The result of this is occurrence of even

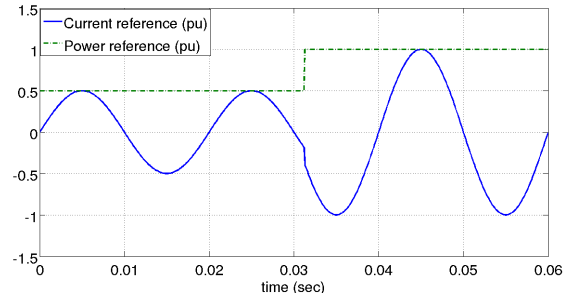

Fig. 3. Occurrence of non-zero average in current reference due to fast changing power reference from MPPT.

harmonics. The dc in the system can be eliminated by using the PRI controller which is discussed next.

B. Fundamental current control

1) Introduction to PRI controller: Conventional stationary reference frame control consists of a PR controller to generate the inverter voltage reference. In this paper, a modification to the PR controller is proposed, by adding an integral block, G_I as indicated in Fig. 4. The modified control structure is termed as PRI controller.

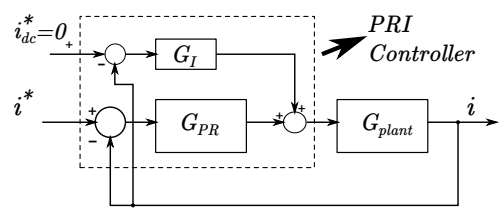

Fig. 4. Block diagram of the fundamental current control with the PRI controller.

Here

$$G_I = \frac{K_I}{s} \tag{2}$$

$$G_{PR}(s) = K_p + \frac{K_r s}{s^2 + \omega_o^2} \tag{3}$$

The plant transfer function is modelled as

$$G_{plant}(s) = \frac{V_{dc}}{R_s + sL_s} \tag{4}$$

This is because the inverter will have a gain of V_{dc} to the voltage reference generated by the controller and the impedance offered is given by $(R_s + sL_s)$ in s-domain. R_s and L_s are the net resistance and inductance referred to the primary side of the transformer respectively. L_s includes the filter inductance and the leakage inductance of the transformer. R_s is the net series resistance due to the filter inductor and the transformer.

The PRI controller is proposed to ensure that the output current of the system does not contain any dc offset. The PRI controller introduces a $zero$ at $s = 0$ in the closed loop transfer function. Hence the output current will not contain any steady state dc offset. This is necessary in the topology considered

because the presence of a dc offset would result in a flow of even harmonics as explained in Section II-A.

The following subsection explains the design of PR controller parameters and proposes a systematic method of selecting and tuning the gain of the integral block in the PRI controller.

2) Design of PRI controller parameters: The fundamental current corresponds to the power injected into the grid. The control objective is to achieve UPF operation of the inverter. The main control block diagram is shown in Fig. 4.

Firstly a PR controller is designed for the system assuming that the integral block is absent i.e., $K_I = 0$. Design of PR controller is done by considering a PI controller in place of the PR controller [36]. The PI parameters are chosen based on the plant transfer function and the required current controller bandwidth. The PI controller parameters are then plugged in for the PR controller parameters.

Let

$$G_{PI}(s) = K_{p1}\frac{1+sT}{sT} \tag{5}$$

With the PI controller as the compensator block in Fig. 4 and without integral block, the forward transfer function will be

$$G_{forw}(s) = \left(K_{p1}\frac{1+sT}{sT}\right)\frac{V_{dc}}{R_s + sL_s} \tag{6}$$

The pole in (6) is cancelled with the zero given by the PI controller. Then the following relations are obtained:

$$T = \frac{L_s}{R_s} \tag{7}$$

$$G_{forw}(s) = \frac{K_{p1}}{sT}\frac{V_{dc}}{R_s} \tag{8}$$

If ω_{bw} is the required bandwidth, then K_{p1} can be chosen to be

$$K_{p1} = \frac{\omega_{bw}R_sT}{V_{dc}} \tag{9}$$

Now if the PI controller in (5) is written as shown below,

$$G_{PI}(s) = K_{p1} + \frac{K_{i1}}{s} \tag{10}$$

Then K_{i1} is given as

$$K_{i1} = \frac{\omega_{bw}R_s}{V_{dc}} \tag{11}$$

For the PR controller, the expressions obtained in (9) and (11) are used for the proportional and resonant gain respectively. Thus

$$K_p = \frac{\omega_{bw}R_sT}{V_{dc}} \tag{12}$$

$$K_r = \frac{\omega_{bw}R_s}{V_{dc}} \tag{13}$$

For the complete system with integral block i.e., the PRI controller, the PR parameters will be same as in (12) and (13).

The following procedure is used to select the value of K_I in (2). The integral portion is used to ensure that there will not be any steady state dc in the system. Hence, the overall dynamic performance of the complete system should be similar to that with the PR controller except at the low frequency region and dc.

The closed loop transfer function for Fig. 4 is given as

$$\begin{aligned} G_{cl,PRI} &= \frac{i(s)}{i^*(s)} \\ &= \frac{G_{plant}G_{PR}}{1+G_{plant}(G_{PR}+G_I)} \end{aligned} \tag{14}$$

Without the integral block, the closed loop transfer function would be

$$G_{cl,PR} = \frac{G_{plant}G_{PR}}{1+G_{plant}G_{PR}} \tag{15}$$

Let (4) be modified as,

$$G_{plant} = \frac{M}{1+sT} \tag{16}$$

Where $M = V_{dc}/R_s$ and T is as defined in (7).

The numerators in both (14) and (15) are the same. Thus the difference in their response is only due to the denominator terms in both. The denominator in (14) can be obtained as,

$$\begin{aligned} den_{PRI} = \Bigg[&\frac{Ts^4 + (1+MK_p)s^3 + (\omega_o^2T + M(K_r+K_I))s^2}{s(1+sT)(s^2+\omega_o^2)} \\ &+ \frac{\omega_o^2(1+MK_p)s + MK_I\omega_o^2}{s(1+sT)(s^2+\omega_o^2)}\Bigg] \end{aligned} \tag{17}$$

Similarly the denominator in (15) is given by,

$$\begin{aligned} den_{PR} = \Bigg[&\frac{Ts^3 + (1+MK_p)s^2 + (\omega_o^2T + MK_r)s}{(1+sT)(s^2+\omega_o^2)} \\ &+ \frac{(MK_p+1)\omega_o^2}{(1+sT)(s^2+\omega_o^2)}\Bigg] \end{aligned} \tag{18}$$

The numerators in (17) and (18) are the characteristic polynomials of the closed loop transfer functions given in (14) and (15) respectively.

Let the numerator polynomial in (17) be written as

$$\begin{aligned} &(s+p)(as^3+bs^2+cs+d) \\ &= as^4 + (b+ap)s^3 + (c+bp)s^2 + (d+cp)s + dp \end{aligned} \tag{19}$$

Where p corresponds to a real pole. Equating (19) with the numerator in (17), the following relations can be obtained.

$$\begin{aligned} a &= T \\ b &= 1 + MK_p - Tp \\ c &= \omega_o^2T + M(K_r+K_I) - (1+MK_p)p - Tp^2 \\ d &= MK_I\omega_o^2/p \end{aligned} \tag{20}$$

If p is such that it is very close to the origin and the remaining three poles in (14) are as close as possible to the poles of (15), then the response in case of PRI controller and PR controller will be very similar except for dc and low frequency range. Thus the remaining third order polynomial in (19) should have the coefficients very close to the coefficients

of the numerator in (18). In that case, using (20) the following conditions can be derived,

$$p << \frac{1 + MK_p}{T} \tag{21}$$

$$K_I < K_r \tag{22}$$

$$K_I = p(K_p + 1/M) \tag{23}$$

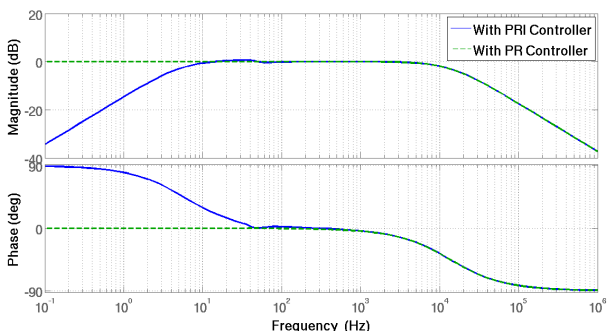

Fig. 5. Comparison of Bode plot of the closed loop transfer function with PRI ($G_{cl,PRI}$) and PR controller ($G_{cl,PR}$).

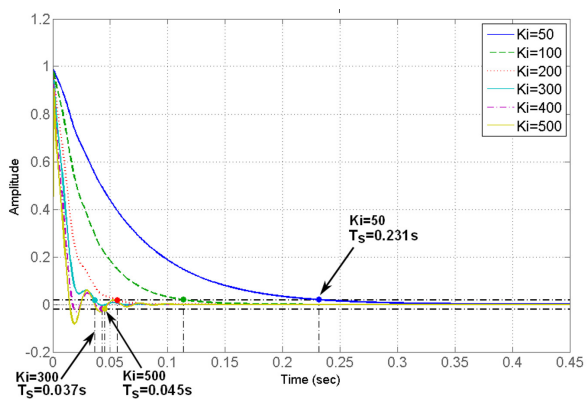

Fig. 6. Step response of closed loop transfer function $G_{cl,PRI}$ for different values of K_I.

Thus (21)–(23) can be used to design the value of K_I. Fig. 5 shows the comparison between the bode plots of the system with PRI and PR controller validating the design procedure for the values given in Table II. As it can be observed, the responses differ only in the low frequency range. The system with PRI controller has zero gain for dc while the system with PR controller has a gain of near unity.

The step response of the closed loop system with PRI controller can be seen in Fig. 6. As can be observed, increasing K_I has an effect of decreasing the settling time upto a certain value. Beyond that the system becomes under damped and settling time increases with increase in K_I. This plot can be used to tune the value of K_I further, after the design from (21)–(23).

III. Adaptive Harmonic Compensation

In this section firstly the LMS adaptive filter is briefly reviewed. Then the concept of lower order harmonic compensation and the design of the adaptive harmonic compensation block using this adaptive filter is explained. Next complete current control along with the harmonic compensation blocks is presented. Finally, the stability considerations are discussed.

A. Review of LMS adaptive filter

The adaptive harmonic compensation technique is based on the usage of a LMS adaptive filter to estimate a particular harmonic in the output current. This is then used to generate a counter voltage reference using a proportional controller to attenuate that particular harmonic.

Adaptive filters are commonly used in signal processing applications to remove a particular sinusoidal interference signal of known frequency [37]. Fig. 7 shows a general adaptive filter with N weights. The weights are adapted by making use of LMS algorithm.

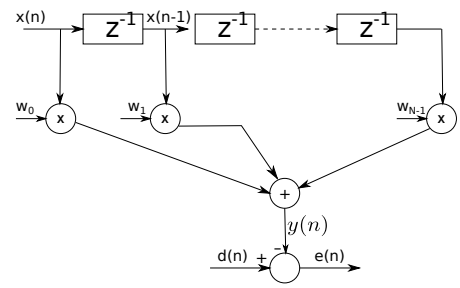

Fig. 7. Structure of a generalized adaptive filter with adaptation weights w_i.

For Fig. 7 coefficient vector is defined as:

$$\overline{w} = [w_o \quad w_1 \quad \ldots \quad w_{N-1}]^T \tag{24}$$

Input vector and filter output are given in (25) and (26).

$$\overline{x}(n) = [x(n) \quad x(n-1) \quad \ldots \quad x(n-N+1)]^T \tag{25}$$

$$y(n) = \overline{w}^T \overline{x}(n) \tag{26}$$

The error signal is,

$$e(n) = d(n) - y(n) \tag{27}$$

Here $d(n)$ is the primary input. A frequency component of $d(n)$ is adaptively estimated by $y(n)$. Now a performance function is defined for LMS adaptive filter as

$$\zeta = e^2(n) \tag{28}$$

In any adaptive filter, the weight vector $\overline{w}$ is updated such that the performance function moves towards its minimum. Thus,

$$\overline{w}(n+1) = \overline{w}(n) - \mu \nabla (e(n)^2) \tag{29}$$

In (29) μ is the step size. The convergence of the adaptive filter depends on the step size μ. A smaller value would make the adaptation process very slow whereas a large value can make the system oscillatory. ∇ is defined as the gradient of the performance function with respect to the weights of the filter.

The final update equation for weights of an LMS adaptive filter can be shown to be as in (30) [37]

$$\overline{w}(n+1) = \overline{w}(n) + 2\mu e(n) \overline{x}(n) \tag{30}$$

Thus from a set of known input vector $\overline{x}(n)$, a signal $y(n)$ is obtained by the linear combination of $\overline{x}(n)$ and the weight vector $\overline{w}(n)$ as in (26). Signal $y(n)$ is an estimate of the signal $d(n)$ and the weight vector is continuously updated from (30) such that the LMS error $e(n) = d(n) - y(n)$ is minimized.

This concept can be used to estimate any desired frequency component in a signal $d(n)$. The adaptive filter used for this purpose will take the reference input $\overline{x}(n)$ as the sine and cosine terms at that desired frequency. The weight vector will contain two components which scale the sine and cosine and add them up to get an estimated signal $y(n)$. The weights will then be adapted in such a way as to minimize the LMS error between $d(n)$ and $y(n)$. In steady state, estimated signal $y(n)$ will equal the frequency component of interest in $d(n)$.

B. Adaptive Harmonic Compensation

LMS adaptive filter discussed previously can be used for selective harmonic compensation of any quantity, say grid current. To reduce a particular lower order harmonic (say i_k) of grid current:

- i_k is estimated from the samples of grid current and phase locked loop (PLL) [38] unit vectors at that frequency.
- A voltage reference is generated from the estimated value of i_k.
- Generated voltage reference is subtracted from the main controller voltage reference.

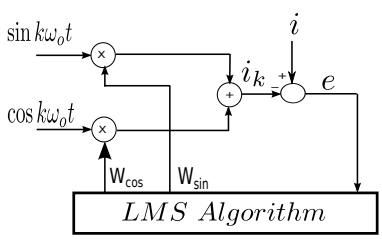

Fig. 8. Block diagram of adaptive estimation of a particular harmonic of grid current.

Fig. 8 shows the block diagram of the adaptive filter that estimates the kth harmonic i_k of the grid current i. The adaptive block takes in two inputs $sin(k\omega_o t)$ and $cos(k\omega_o t)$ from PLL. These samples are multiplied by the weights W_{cos} and W_{sin}. The output is subtracted from the sensed grid current sample, which is taken as the error for LMS algorithm. The weights are then updated as per LMS algorithm and the output of this filter would be an estimate of the kth harmonic of grid current.

The weights update would be done by using the equations given below, where T_s is the sampling time, $e(n)$ is the error of nth sample and μ is the step size:

$$e(n) = i(n) - i_k(n) \quad (31)$$

$$W_{cos}(n+1) = W_{cos}(n) + 2\mu e(n) cos(k\omega_o n T_s) \quad (32)$$

$$W_{sin}(n+1) = W_{sin}(n) + 2\mu e(n) sin(k\omega_o n T_s) \quad (33)$$

Now a voltage reference has to be generated from this estimated current. In this work, the proportional gain method is used as it is very simple for both design and implementation and is verified to meet harmonic requirements. Fig. 9 shows the scheme used for harmonic voltage reference generation from estimated harmonic current.

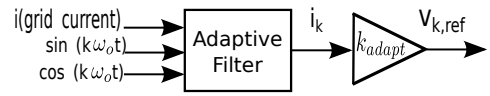

Fig. 9. Generation of voltage reference from estimated k^{th} harmonic component of current using the LMS adaptive filter.

The overall current control block diagram with the adaptive compensation is shown in Fig. 10. Note that the fundamental current control is done using the transformer primary current and the harmonic compensation block uses the secondary current, which is the current injected into the grid.

Fig. 10 shows only one adaptive harmonic compensation block for the kth harmonic. If say dominant harmonics third, fifth and seventh need to be attenuated, then three adaptive filters and three gain terms k_{adapt} are required and the net voltage reference added to the output of the PRI controller will be the sum of the voltage references generated by each of the block. Thus depending on the number of harmonics to be attenuated, the number of blocks can be selected.

Note that n in Fig. 10 is the transformer turns ratio from secondary to primary. $i_{sec,k,t}$ is the net k^{th} harmonic current in the secondary, which is estimated using the LMS adaptive filter. This is mainly due to the harmonics in the magnetizing current and the dead-time effect. A single phase PLL is used to generate the reference sine-cosine signals synchronized with the grid voltage for the adaptive filter. Next, computation of the adaptive gain k_{adapt} is discussed.

1) Computation of k_{adapt}: Based on the estimated net k^{th} harmonic in the grid current, the voltage reference $v_{k,ref}$ is generated by multiplying the estimated harmonic with k_{adapt}. The effect of this voltage reference is that it results in an amplified voltage at that harmonic frequency at the inverter terminals and this will inject a current at that frequency in the primary side. The reflected secondary current will oppose the original current that was present in the secondary and hence there will be a net reduction in that particular harmonic in the grid current. Consequently, the primary side current will be more distorted. The amount of reduction of the harmonic in grid current will depend on k_{adapt}.

To calculate k_{adapt}, the control block diagram shown in Fig. 11 is used. This block diagram is derived using Fig. 10 by considering the control variable to be regulated as the kth harmonic in secondary current. While deriving this harmonic control block diagram, the fundamental reference i^*_{pri} is set to zero and $G_{PRI} = G_{PR} + G_I$. Here $i_{pri,k}$ is the kth harmonic in primary current, $i_{sec,k}$ is the corresponding reflected secondary current. The net k^{th} harmonic in the secondary is given by $i_{sec,k} - i_{sec,k(0)}$, which is estimated by the adaptive filter to give $i_{sec,k,t}$. $i_{sec,k(0)}$ is the kth harmonic current flowing when there was no compensation.

Let $G(s)$ be the transfer function between $v_{k,ref}$ and $i_{pri,k}$. This can be expressed from Fig. 11 as in (34). Here $G_{plant}(s)$

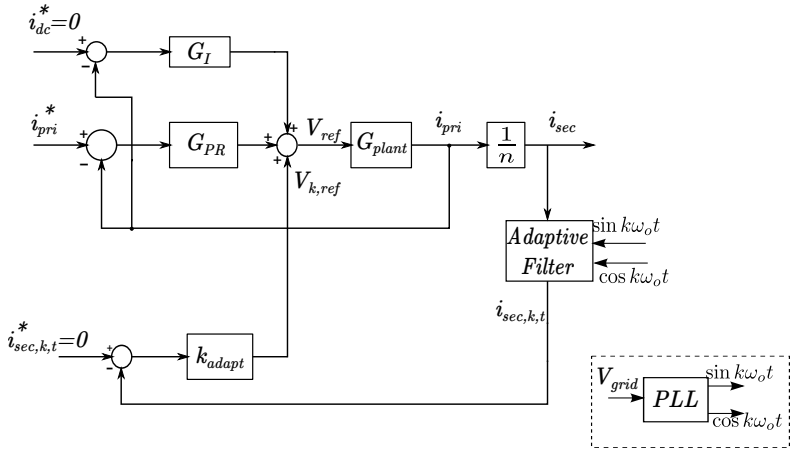

Fig. 10. Complete ac current control structure of the inverter.

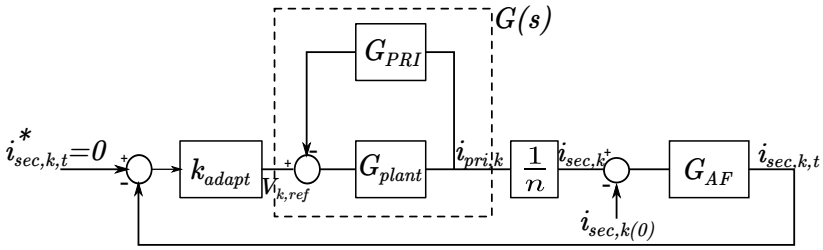

Fig. 11. Block diagram for calculating k_{adapt}.

is the plant transfer function as given in (4).

$$G(s) = \frac{G_{plant}(s)}{1 + G_{plant}(s)G_{PRI}(s)} \tag{34}$$

$G_{AF}(s)$ is the equivalent transfer function of the adaptive filter tracking k^{th} harmonic of the grid current. In order to model $G_{AF}(s)$, consider an adaptive filter which tracks a dc value in a signal. This dc tracking adaptive filter can be modelled as a first order transfer function with unity gain and with a time constant T_a which depends on the parameter μ. This transfer function is designated as $G_{AF,0}(s)$ and is given in (35). In order to obtain the transfer function of the adaptive filter tracking k^{th} harmonic, low pass to bandpass transformation [36] is used to transform (35). This gives $G_{AF}(s)$ as in (36).

$$G_{AF,0}(s) = \frac{1}{1 + sT_a} \tag{35}$$

$$G_{AF}(s) = \frac{2s}{T_a s^2 + 2s + (k\omega_o)^2 T_a} \tag{36}$$

Thus

$$\frac{i_{sec,k,t}}{i^*_{sec,k,t}}(s) = \frac{k_{adapt}G(s)G_{AF}(s)/n}{1 + k_{adapt}G(s)G_{AF}(s)/n} \tag{37}$$

For the kth harmonic, let the steady value for the transfer function in (37), evaluated at frequency $k\omega_o$ have a magnitude α, with $\alpha < 1$. Then

$$|\frac{i_{sec,k,t}}{i^*_{sec,k,t}}(jk\omega_o)| = \alpha \tag{38}$$

$$|\frac{k_{adapt}G(jk\omega_o)G_{AF}(jk\omega_o)/n}{1 + k_{adapt}G(jk\omega_o)G_{AF}(jk\omega_o)/n}| = \alpha \tag{39}$$

As $G_{AF}(jk\omega_o) = 1$,

$$k_{adapt} = \frac{\alpha}{1-\alpha}\frac{n}{|G(jk\omega_o)|} \tag{40}$$

The transfer function $G(jk\omega_o)$ for harmonics can be approximated as

$$|G(jk\omega_o)| \approx \frac{1}{|G_{PRI}(jk\omega_o)|}$$
$$\Rightarrow |G(jk\omega_o)| \approx \frac{1}{K_p} \tag{41}$$

Using (41) in (40), the final expression for k_{adapt} can be obtained as

$$k_{adapt} = \frac{\alpha}{1-\alpha} n K_p \tag{42}$$

For a given value of $\alpha < 1$, it can be shown that, the original k^{th} harmonic in the grid current gets reduced by a factor of $1/(1-\alpha)$. Thus k_{adapt} can be chosen from (42) depending on the amount of reduction required. The residual distortion after adaptive compensation can be determined as,

$$i_{sec,k,t} = i_{sec,k(0)} \times (1-\alpha) \tag{43}$$

C. Interaction between the PRI controller and Adaptive Compensation Scheme

It can be recalled that while designing K_p, K_r and K_I, the control block diagram considered in Fig. 4 did not include the effect of adaptive compensation. In fact, from Fig. 10, it can be observed that the primary current control is linked to the adaptive compensation section and the actual transfer

TABLE I
COEFFICIENTS IN THE PRIMARY CURRENT CONTROL TRANSFER FUNCTION $G_{cl,a}$.

Coefficient	Value	Coefficient	Value
		a_6	151×10^{-6}
b_5	12.86	a_5	12.9
b_4	3403	a_4	$3982 + 19.05k_{adapt}$
b_3	1.286×10^7	a_3	1.297×10^7
b_2	2.346×10^9	a_2	$10^6(2782 + 1.880k_{adapt})$
b_1	1.127×10^{12}	a_1	1.133×10^{12}
		a_0	3.757×10^{13}

function for the primary current control including the model for adaptive compensation is as given below:

$$G_{cl,a} \triangleq \frac{i_{pri}}{i^*_{pri}} = \frac{G_{PR}G_{plant}}{1 + G_{plant}(G_{PR} + G_I + G_{AF}k_{adapt}/n)} \quad (44)$$

To ensure that the fundamental control loop performance is not affected appreciably, the bode plots of the transfer function $G_{cl,a}$ given in (44) and the one used in (14) are compared. Fig. 12 shows the two bode plots for the design values as in Table II. As it can be observed, there is no appreciable difference in the two plots.

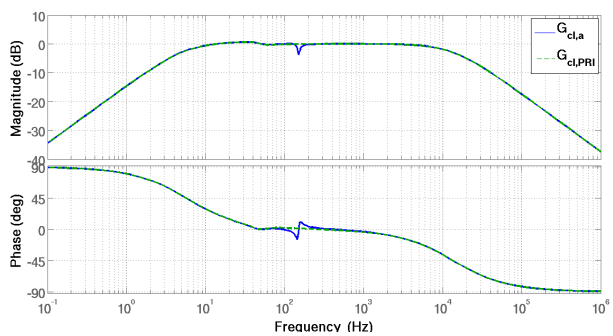

Fig. 12. Comparison of approximate and actual fundamental inverter ac current control transfer function for $T_a = 0.03s$, $k_{adapt} = 25.6$.

Note that the extra term appearing in the actual transfer function will modify the overall response near the harmonic frequency range, third harmonic in Fig. 12. At all other frequency range the response is practically same.

As the value of k_{adapt} determines the amount of compensation, the stability of the closed loop transfer function is analysed as k_{adapt} varies. This is done by looking at the Routh array of the denominator polynomial in the closed loop transfer function as given in (44). Now (44) as a function of k_{adapt} is determined by the transfer function,

$$G_{cl,a} = \frac{b_5s^5 + b_4s^4 + b_3s^3 + b_2s^2 + b_1s}{a_6s^6 + a_5s^5 + a_4s^4 + a_3s^3 + a_2s^2 + a_1s + a_0} \quad (45)$$

The coefficients in (45) are provided in Table I.

The first column elements of Routh array for the denominator in (45) are given below,

$$\begin{pmatrix} 151.1 \times 10^{-6} \\ 12.9 \\ 3830 + 19.05k_{adapt} \\ \frac{222.8\times10^6 k_{adapt} + 1.39\times10^{10}}{3830 + 19.05k_{adapt}} \\ \frac{7.8\times10^{12}k_{adapt}^2 + 4.9\times10^{17}k_{adapt} + 2.4\times10^{19}}{222.8\times10^6 k_{adapt} + 1.39\times10^{10}} \\ \frac{7\times10^{17}k_{adapt}^2 + 3.6\times10^{22}k_{adapt} + 1.8\times10^{24}}{6.2\times10^5 k_{adapt}^2 + 3.9\times10^{10}k_{adapt} + 1.9\times10^{12}} \\ 3.757 \times 10^{13} \end{pmatrix} \quad (46)$$

As can be observed from (46), there is no sign change in the first column for positive k_{adapt}. This means that the system will be stable for all positive values of k_{adapt}, which is selected using (42). Thus the interaction between the PRI loop and adaptive compensation scheme would not affect the stability of the system, and also as observed from Fig. 12 the response for the design values is practically unaffected.

IV. EXPERIMENTAL RESULTS

A. System Parameters

The circuit topology shown in Fig. 1 was built in the laboratory for a maximum power rating of 150W. The power circuit and control parameters are listed in Table II. All the design related plots and the experimental results have the parameters as listed in Table II.

B. Description of the Hardware

The photograph of the experimental set up of the laboratory built prototype converter is shown in Fig. 13. The photograph shows the main circuit board which contains the power circuit, the filter inductor, the line frequency grid interface transformer and the FPGA based controller board. A sensor interface circuit board is stacked below the main circuit board PCB. In addition to the power circuit, the main circuit board contains gate drive circuit, protection and dead-time generation circuits. The protection circuit will shut-down the operation during abnormal conditions such as over current, under voltage etc. The gate drive circuit is designed using the gate driver IC IR2110.

The controller board used consists of an Altera EP1C12Q240C8 FPGA chip as the digital platform for control implementation. The complete current control proposed in this paper is implemented in this FPGA chip. Transformer primary and secondary currents are sensed and input to the FPGA using A/D converters for the complete current control. The outputs from the controller are the PWM pulses which are generated using sine-triangle PWM technique for the voltage reference computed within the FPGA. The control algorithm is implemented in VHDL.

As mentioned in Section I, the proposed current control is simple and consumes less resources in the digital controller. To quantify this, the number of multiplications and additions required in the implementation of the proposed technique is compared with two other popular harmonic elimination techniques namely the PR+multiresonant based as in [19]–[22] and the PR+adaptive LMS+multiresonant based techniques

TABLE II
PV INVERTER PARAMETERS.

Parameter	Meaning	Value/Part Number
V_{dc}	DC bus voltage	40V
1:n	Transformer turns ratio	1:15
ω_{bw}	Bandwidth of current controller	84.8×10^3 rad/s
R_s	Net series resistance referred to primary	0.28Ω
L_s	Net series inductance referred to primary	$1.41mH$
$S_1 - S_4,\ S_{boost}$	Power MOSFETs	IRF Z44 ($V_{DS,max} = 60V$, $I_{D,max} = 50A$)
C_{dc}	DC bus capacitance	$6600\mu F, 63V$
f_{sw}	Device switching frequency	$40kHz$
K_p	Proportional term	3
K_r	Resonant term	594
K_I	Integral term	100
K_{adapt}	Gain in harmonic compensation block	25.6
T_a	Time constant in $G_{AF,0}(s)$ and $G_{AF}(s)$	0.03s

as in [27]. It is considered that the resonant controllers at harmonic frequency for these two techniques are implemented as indicated in [21] to assure adequate performance and resonance frequency adaptability. However, the fundamental PR controller implementation in all the three cases is assumed to be done using bilinear transformation for discretization of the PR controller transfer function.

The result of the comparison is given in Table III which shows the number of multiplications and additions required for the fundamental current control and control of one harmonic, say third harmonic. For multiple harmonic control, the numbers mentioned there would increase linearly. As given in Table III, the proposed method has higher resource requirement for the fundamental current control as it uses an integral block in addition to the fundamental PR controller. But it can be observed that the resource utilization is lesser for the proposed method in the harmonic current control case. Thus it can be observed from Table III that overall the proposed method uses less resources.

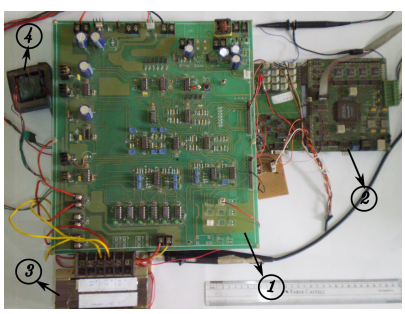

Fig. 13. Hardware setup at laboratory showing main circuit board (1), FPGA controller board (2), line frequency transformer (3) and filter inductor (4).

C. Experimental Results

This section contains the experimental results validating the design procedure proposed in this paper. All the experimental results correspond to one of the four cases of current control that are listed in Table IV.

Case 1 has just a PR controller and will have highest lower order harmonic distortion. Case 2 contains PR controller and adaptive harmonic compensation. Case 3 contains only PRI controller but the LMS adaptive filter is disabled. Case 4 contains both the methods proposed in this paper i.e., PRI controller and adaptive harmonic compensation using LMS filter and proportional controller. This case will have the least lower order harmonic distortion.

First set of experimental results are shown in Fig. 14, Fig. 15 and Fig. 16. Here the control loop does not have a dc offset and hence the grid current does not contain any significant even harmonics. The distortion is due to the lower order odd harmonics caused predominantly by the distorted transformer magnetizing current.

Fig. 14(a) shows the grid current and sensed grid voltage with voltage sensor gain of $0.01V/V$ for current control method of case 1 as indicated in Table IV. The presence of lower order harmonics can be seen from Fig. 14(a). The Fig. 14(b) shows the same set of waveforms when the proposed control scheme is used, which corresponds to case 4 with adaptive compensation applied to third harmonic alone. The improvement in the wave-shape can be observed due to the attenuation of the third harmonic.

The harmonic spectrum of the grid current waveform in Fig. 14 is shown in Fig. 15. The reduction in the third harmonic can be observed from the spectrum in Fig. 15. The summary of the THD of the grid current waveform in Fig. 14 is given in Table V. As mentioned in the Table V, the THD in the grid current has been brought to less than 5% by just using third harmonic compensation. The third harmonic was reduced from a value of 7.38% to 3.47%. If necessary, by adding adaptive compensation blocks for the higher harmonics the THD of grid current can be further improved.

TABLE V
COMPARISON OF GRID CURRENT THD AND ITS THIRD HARMONIC CONTENT FOR CASE 1 AND CASE 4 WHEN THERE IS NO DC OFFSET IN THE CONTROL LOOP.

Quantity	Without compensation (Case 1)	With compensation (Case2)
Grid current THD	8.20%	4.97%
Magnitude of third harmonic	7.34%	3.47%

For the same situation, Fig. 16 shows the primary current and the sensed grid voltage. Primary current for case 1 is of a better quality, as can be seen from Fig. 16(a). This is because the dominant cause for distortion in this system is the distorted transformer magnetizing current. This was drawn from the grid

TABLE III
COMPARISON OF THE NUMBER OF MULTIPLICATIONS AND ADDITIONS REQUIRED FOR THE IMPLEMENTATION OF PROPOSED CONTROL TECHNIQUE, MULTIRESONANT BASED TECHNIQUE AND ADAPTIVE PLUS MULTIRESONANT BASED TECHNIQUE.

Method	*Fundamental current control*		*Harmonic current control*		*Total*	
	Multiplications	Additions	Multiplications	Additions	Multiplications	Additions
PR+multiresonant	4	4	9	8	13	12
PR+LMS adaptive+multiresonant	4	4	13	13	17	17
Proposed Method	**5**	**6**	**5**	**5**	**10**	**11**

TABLE IV
FOUR CASES OF INVERTER CURRENT CONTROL.

Case 1	No dc offset compensation and no adaptive harmonic compensation
Case 2	No dc offset compensation but adaptive harmonic compensation is implemented
Case 3	DC offset compensation is implemented but no adaptive harmonic compensation
Case 4	Both dc offset compensation and adaptive harmonic compensation are implemented

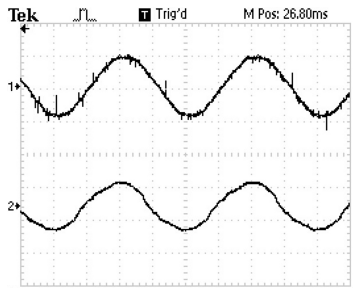

(a)

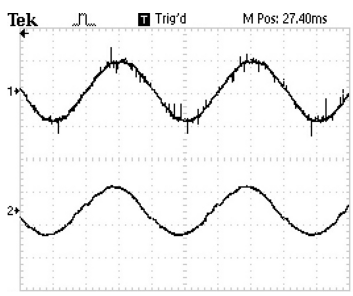

(b)

Fig. 14. Comparison of grid current when there is no dc offset in control loop - (a) Case 1: No dc offset compensation and no adaptive harmonic compensation (b) Case 4: Both dc offset compensation and adaptive harmonic compensation are implemented. [CH2: Grid current (Scale: 1div=1A); CH1: Sensed grid voltage (Scale: 1div=5V), Horizontal scale: 1div=5ms.]

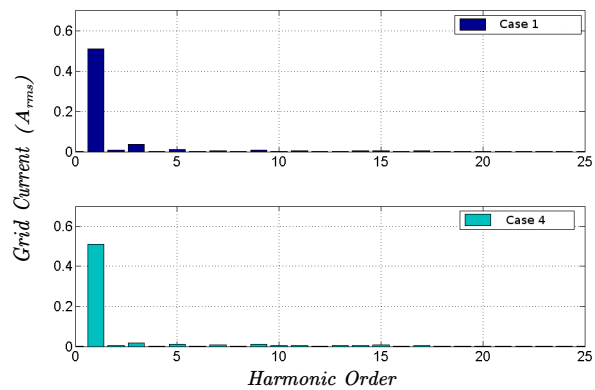

Fig. 15. Comparison of grid current harmonic spectrum for Case 1: No dc offset compensation and no adaptive harmonic compensation and Case 4: Both dc offset compensation and adaptive harmonic compensation are implemented; when there is no dc offset in control loop.

in case 1. From Fig. 16(b) it is clear that the harmonics are added to the primary current and it is more distorted. In other words, the distortion has been transferred from the grid current to the primary side current, which improves the grid current as seen in Fig. 14(b).

The control loop was not having any offset for the results shown in Fig. 14 – Fig. 15. In other words, the performance would have been same even when PR controller were used in place of the proposed PRI controller. To show the effectiveness of the PRI controller, an offset was added to the control loop. As explained in Section II this offset will introduce even harmonics in the grid current. Thus the next set of waveforms shown in Fig. 17 and Fig. 18 are for the case when the control loop contains a dc offset. Here the distortion in the uncompensated case i.e., case 1 is very pronounced due to the presence of significant even harmonics in addition to the odd harmonics as can be seen in Fig. 17(a). The Fig. 17(b) shows the grid current for the same situation but with full compensation i.e., case 4. It can be clearly seen that the Fig. 17(a) has even harmonics whereas in Fig. 17(b) the even harmonics are practically negligible. This is confirmed in the spectrum of grid current shown in Fig. 18. In Table VI, the dc in primary current is compared when the primary current control loop has a dc offset. As it can be observed, the PRI controller practically eliminates the dc component.

TABLE VI
COMPARISON OF DC COMPONENT IN PRIMARY CURRENT WHEN THE PRIMARY CURRENT CONTROL LOOP HAS A DC OFFSET.

Quantity	DC component	
	With PR Controller	With PRI Controller
Primary current	10.22%	0.0159%

The transient response of the system is also studied experimentally by considering the start up transient. Fig. 19(a) shows the transient response of the primary current for case 1 i.e., with PR controller alone and Fig. 19(b) shows the transient response for case 3 i.e., with PRI controller alone. As it can be observed from Fig. 19, the start-up transient is practically same for both PR and PRI controller, which would also assert

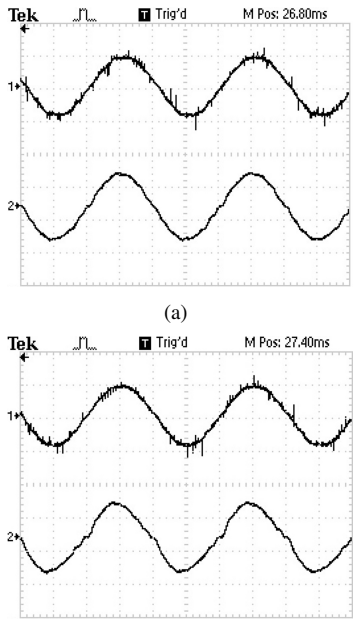

Fig. 16. Comparison of primary current - (a) Case 1: No dc offset compensation and no adaptive harmonic compensation (b) Case 4: Both dc offset compensation and adaptive harmonic compensation are implemented. [CH2: Primary current (Scale: 1div=10A); CH1: Sensed grid voltage (Scale: 1div=5V), Horizontal scale: 1div=5ms.]

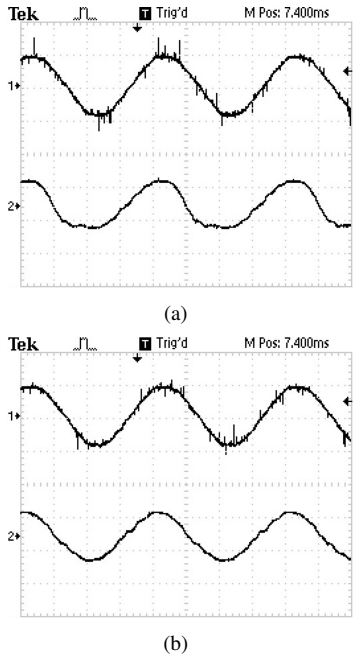

Fig. 17. Comparison of grid current when there is a dc offset in control loop - (a) Case 1: No dc offset compensation and no adaptive harmonic compensation (b) Case 4: Both dc offset compensation and adaptive harmonic compensation are implemented. [CH2: Grid current (Scale: 1div=1A); CH1: Sensed grid voltage (Scale: 1div=5V), Horizontal scale: 1div=5ms.]

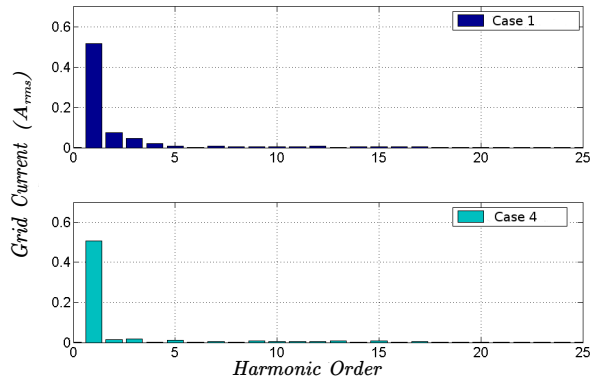

Fig. 18. Comparison of grid current harmonic spectrum for Case 1: No dc offset compensation and no adaptive harmonic compensation, and Case 4: Both dc offset compensation and adaptive harmonic compensation are implemented; when there is a dc offset in control loop.

that the design procedure used for PRI controller meets its objectives. The correction of a dc offset occurs in about three line cycles in case of PRI controller.

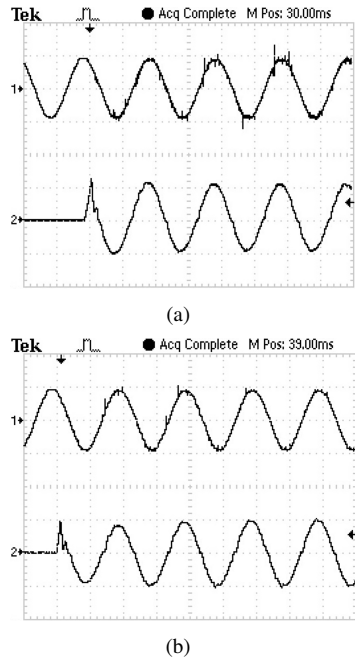

Fig. 19. Startup transient response of the primary current - (a) Case 1: No dc offset compensation and no adaptive harmonic compensation and (b) Case 3: DC offset compensation is implemented but no adaptive harmonic compensation. [CH2: Primary current (Scale: 1div=10A); CH1: Sensed grid voltage (Scale: 1div=5V), Horizontal scale: 1div=10ms.]

Fig. 20(a) shows the start up transient for case 2 and Fig. 20(b) shows the same for case 4. It can be concluded that, the inclusion of adaptive compensation has practically no effect on the main control loop as was deduced using the Bode plot shown in Fig. 12. Thus the transient response of the system with PRI controller and the adaptive compensation is as per the theoretical expectation.

The seamless transition in the grid current can be observed from Fig. 21. Here, when the enable signal is made high, the adaptive compensation and the integrator of the PRI controller

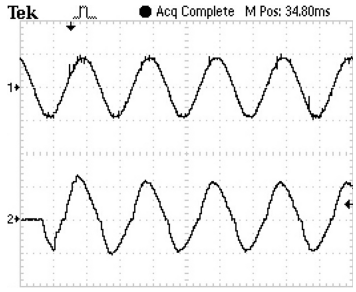

(a)

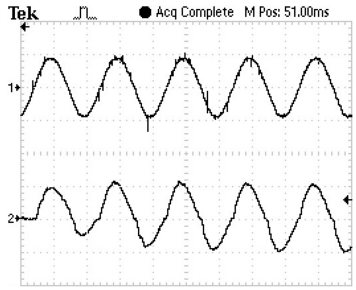

(b)

Fig. 20. Startup transient response of the primary current - (a) Case 2: No dc offset compensation but adaptive harmonic compensation is implemented, (b) Case 4: Both dc offset compensation and adaptive harmonic compensation are implemented. [CH2: Primary current (Scale: 1div=10A); CH1: Sensed grid voltage (Scale: 1div=5V), Horizontal scale: 1div=10ms.]

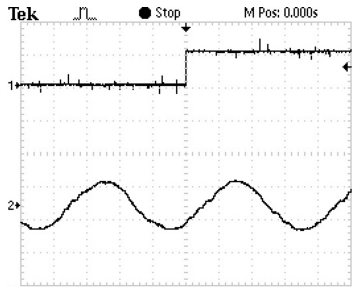

Fig. 21. Smooth transition in the grid current when control algorithm switches over from Case 1 to Case 4. [CH1: Enable (1div=5V), CH2: Grid current(1div=1A), Horizontal scale: 1div=5ms.]

are enabled i.e., a switch over from case 1 to case 4 occurs. This switch over does not produce any abrupt transients in the output current. The smooth transition of the wave shape can be observed from Fig. 21.

The Fig. 22 shows the output of an adaptive filter estimating the third harmonic in the primary current. As it can be observed, the third harmonic content in the primary current increases after the compensation has been enabled. The building up of the output in the LMS adaptive filter can be observed from this figure to occur in about 30ms.

V. Conclusion

Modification to the inverter current control for a grid connected single phase photovoltaic inverter has been proposed in this paper, for ensuring high quality of the current injected into the grid. For the power circuit topology considered, the dominant causes for lower order harmonic injection are identified as the distorted transformer magnetizing current and

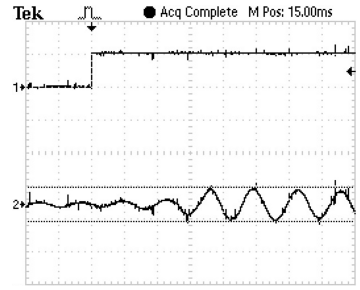

Fig. 22. Transient building up of the output of LMS adaptive filter estimating third harmonic in primary current. [CH1: Enable (1div=5V), CH2: Third harmonic in primary current estimated by LMS adaptive filter(1div=1A), Horizontal scale: 1div=5ms.]

the dead-time of the inverter. It is also shown that the presence of dc offset in control loop results in even harmonics in the injected current for this topology due to the dc biasing of the transformer. A novel solution is proposed to attenuate all the dominant lower order harmonics in the system. The proposed method uses an LMS adaptive filter to estimate a particular harmonic in the grid current that needs to be attenuated. The estimated current is converted into an equivalent voltage reference using a proportional controller and added to the inverter voltage reference. The design of the gain of proportional controller to have an adequate harmonic compensation has been explained. To avoid dc biasing of the transformer, a novel PRI controller has been proposed and its design has been presented. The interaction between the PRI controller and the adaptive compensation scheme has been studied. It is shown that there is minimal interaction between the fundamental current controller and the methods responsible for dc offset compensation and adaptive harmonic compensation. The PRI controller and the adaptive compensation scheme together improve the quality of the current injected into the grid.

The complete current control scheme consisting of the adaptive harmonic compensation and PRI controller has been verified experimentally and the results show good improvement in the grid current THD once the proposed current control is applied. The transient response of the whole system is studied by considering the start up transient and the overall performance is found to agree with the theoretical analysis. It may be noted here that these methods can be used for other applications that use a line interconnection transformer wherein the lower order harmonics have considerable magnitude and need to be attenuated.

References

[1] S. B. Kjaer, J. K. Pedersen, and F. Blaabjerg, “A review of single-phase grid-connected inverters for photovoltaic modules,” *IEEE Trans. Ind. Appl.*, vol. 41, no. 5, pp. 1292-1306, Sept./Oct. 2005.

[2] S. -G. Jeung and M. -H. Park, “The analysis and compensation of dead-time effects in PWM inverters,” *IEEE Trans. Ind. Electron.*, vol. 38, no. 2, pp. 108-114, Apr. 1991.

[3] J. -W. Choi and S. -K. Sul, “A new compensation strategy reducing voltage/current distortion in PWM VSI systems operating with low output voltages,” *IEEE Trans. Ind. Appl.*, vol. 31, no. 5, pp. 1001-1008, Sept./Oct. 1995.

[4] A. R. Muñoz, and T. A. Lipo, “On-line dead-time compensation technique for open-loop PWM-VSI drives,” *IEEE Trans. Power Electron.*, vol. 14, no. 4, pp. 683-689, Jul. 1999.

[5] A. C. Oliveira, C. B. Jacobina, and A. M. N. Lima, "Improved dead-time compensation for sinusoidal PWM inverters operating at high switching frequencies," *IEEE Trans. Ind. Electron.*, vol. 54, no. 4, pp. 2295-2304, Aug. 2007.

[6] L. Chen and F. Z. Peng, "Dead-time elimination for voltage source inverters," *IEEE Trans. Power Electron.*, vol. 23, no. 2, pp. 574-580, Mar. 2008.

[7] *IEEE Recommended Practices and Requirements for Harmonic Control in Electrical Power Systems*, IEEE Standard 519-1992.

[8] *IEEE Standard for Interconnecting Distributed Resources With the Electric Power System*, IEEE Standard 1547-2003.

[9] T. Esram and P. L. Chapman, "Comparison of photovoltaic array maximum power point tracking techniques," *IEEE Trans. Energy Conversion*, vol. 22, no. 2, pp. 439-449, Jun. 2007.

[10] R. Kadri, J-P Gaubert, and G. Champenois, "An improved maximum power point tracking for photovoltaic grid-connected inverter based on voltage-oriented control," *IEEE Trans. Ind. Electron.*, vol. 58, no. 1, pp. 66-75, Jan. 2011.

[11] T. Kitano, M. Matsui, and D Xu, "Power sensorless MPPT control scheme utilizing power balance at DC link - System design to ensure stability and response," in *Proc. 27th Annu. Conf. IEEE Ind. Electron. Soc.*, 2001, pp. 1309-1314.

[12] Y. Chen and K. M. Smedley, "A cost-effective single-stage inverter with maximum power point tracking," *IEEE Trans. Power Electron.*, vol. 19, no. 5, pp. 1289-1294, Jun. 2004.

[13] Q. Mei, M. Shan, L. Liu, and J. M. Guerrero, "A novel improved variable step-size incremental-resistance MPPT method for PV systems," *IEEE Trans. Ind. Electron.*, vol. 58, no. 6, pp. 2427-2434, Jun. 2011.

[14] A. K. Abdelsalam, A. M. Massoud, S. Ahmed, and P. N. Enjeti, "High-performance adaptive perturb and observe MPPT technique for photovoltaic-based microgrids," *IEEE Trans. Power Electron.*, vol. 26, no. 4, pp. 1010-1021, Apr. 2011.

[15] P. Mattavelli, "A closed-loop selective harmonic compensation for active filters" *IEEE Trans. Ind. Appl.*, vol. 37, no. 1, pp. 81-89, Jan./Feb. 2001.

[16] X.Yuan, W. Merk, H. Stemmler, and J. Allmeling, "Stationary-frame generalized integrators for current control of active power filters with zero steady-state error for current harmonics of concern under unbalanced and distorted operating conditions," *IEEE Trans. Ind. Appl.*, vol. 38, no. 2, pp. 523-532, Mar./Apr. 2002.

[17] J. Allmeling, "A control structure for fast harmonics compensation in active filters," *IEEE Trans. Power Electron.*, vol. 19, no. 2, pp. 508-514, Mar. 2004.

[18] C. Lascu, L. Asiminoaei, I. Boldea, and F. Blaabjerg, "High performance current controller for selective harmonic compensation in active power filters," *IEEE Trans. Power Electron.*, vol. 22, no. 5, pp. 1826-1835, Sept. 2007.

[19] D. De and V. Ramanarayanan, "A proportional + multiresonant controller for three-phase four-wire high-frequency link inverter," *IEEE Trans. Power Electron.*, vol. 25, no. 4, pp. 899-906, Apr. 2010.

[20] R. Cárdenas, C. Juri, R. Peña, P. Wheeler, and J. Clare, "The application of resonant controllers to four-leg matrix converters feeding unbalanced or nonlinear loads," *IEEE Trans. Power Electron.*, vol. 27, no. 3, pp. 1120-1128, Mar. 2012.

[21] A. G. Yepes, F. D. Freijedo, Ó. López, and J. Doval-Gandoy, "High-performance digital resonant controllers implemented with two integrators," *IEEE Trans. Power Electron.*, vol. 26, no. 2, pp. 563-576, Feb. 2011.

[22] A. G. Yepes, F. D. Freijedo, J. Doval-Gandoy, O. Lopez, J. Malvar, and P. Fernandez-Comesaña , "Effects of discretization methods on the performance of resonant controllers," *IEEE Trans. Power Electron.*, vol. 25, no. 7, pp. 1692-1712, Jul. 2010.

[23] P. Mattavelli and F. P. Marafao, "Repetitive-based control for selective harmonic compensation in active power filters," *IEEE Trans. Ind. Electron.*, vol. 51, no. 5, pp. 1018-1024, Oct. 2004.

[24] R. Costa-Costello, R. Grino, and E. Fossas, "Odd-harmonic digital repetitive control of a single-phase current active filter," *IEEE Trans. Power Electron.*, vol. 19, no. 4, pp. 1060-1068, Jul. 2004.

[25] S. Jiang, D. Cao, Y. Li, J. Liu, and F. Z. Peng, "Low-THD, fast-transient, and cost-effective synchronous-frame repetitive controller for three-phase UPS inverters," *IEEE Trans. Power Electron.*, vol. 27, no. 6, pp. 2994-3005, Jun. 2012.

[26] J. M. Olm, G. A. Ramos, and R. Costa-Costeló, "Stability analysis of digital repetitive control systems under time-varying sampling period," *IET Control Theory Appl.*, vol. 5, Iss. 1, pp. 29-37, 2011.

[27] M. Cirrincione, M. Pucci, G. Vitale, and A. Miraoui, "Current harmonic compensation by a single-phase shunt active power filter controlled by adaptive neural filtering," *IEEE Trans. Ind. Electron.*, vol. 56, no. 8, pp. 3128-3143, Aug. 2009.

[28] B. Singh and J. Solanki, "An implementation of an adaptive control algorithm for a three-phase shunt active filter," *IEEE Trans. Ind. Electron.*, vol. 56, no. 8, pp. 2811-2820, Aug. 2009.

[29] L. Qian, D. A. Cartes, and H. Li, "An improved adaptive detection method for power quality improvement," *IEEE Trans. Ind. Appl.*, vol. 44, no. 2, pp. 525-533, Mar./Apr. 2008.

[30] S. -Y. Kim and S. -Y. Park, "Compensation of dead-time effects based on adaptive harmonic filtering in the vector-controlled AC motor drives" *IEEE Trans. Ind. Electron.*, vol. 54, no. 3, pp. 1768-1777, Jun. 2007.

[31] V. Blasko, "A novel method for selective harmonic elimination in power electronic equipment," *IEEE Trans. Power Electron.*, vol. 22, pp. 223-228, 2007.

[32] A. E. Fitzgerald, Charles Kingsley Jr., and Stephen D. Umans, "Electric Machinery," Sixth Ed., McGraw Hill, 2003.

[33] J. D. Aspnes, R. P. Merritt, and S.I. Akasofu, "Harmonic generation in transformers related to DC excitation and system loading," *IEEE Trans. Power App. Sys.*, vol. PAS100, no. 4, pp. 1845-1851, Apr. 1981.

[34] S. Lu, Y. Liu and J. De La Ree, "Harmonics generated from a DC biased transformer," *IEEE Trans. Power Del.*, vol. 8, no. 2, pp. 725-731, Apr. 1993.

[35] J. A. Orr and A. E. Emanuel, "On the need for strict second harmonic limits," *IEEE Trans. Power Del.*, vol. 15, no. 3, pp. 967-971, Jul. 2000.

[36] D. N. Zmood and D. G. Holmes, "Stationary frame current regulation of PWM inverters with zero steady-state error," *IEEE Trans. Power Electron.*, vol. 18, no. 3, pp. 814-822, May 2003.

[37] J. R. Glover. Jr, "Adaptive noise cancelling applied to sinusoidal interferences," *IEEE Trans. Acoust., Speech, Signal Process.*, vol. 25, no. 6, pp. 484-491, Dec. 1977.

[38] M. Ciobotaru, R. Teodorescu, and F. Blaabjerg, "A new single phase PLL structure based on second order generalized integrator," in *Proc. 37th IEEE Power Electron. Spec. Conf.*, June 2006, pp. 1-6.

Abhijit Kulkarni (S'05) received the B.Tech. degree in electrical and electronics engineering from the National Institute of Technology, Calicut, India, in 2009, and the M.E. degree in electrical engineering in 2011 from the Indian Institute of Science, Bangalore, India, where currently he is working towards the Ph.D. degree from the Department of Electrical Engineering.

His current research interests include power electronics for renewable energy systems, grid connected power converters and power quality issues.

Vinod John (S'92-M'00-SM'09) received the B.Tech. degree in electrical engineering from the Indian Institute of Technology, Madras, India, the M.S.E.E. degree from the University of Minnesota, Minneapolis, and the Ph.D. degree from the University of WisconsinMadison, Madison.

He has worked in research and development positions at GE Global Research, Niskayuna, NY, and Northern Power, VT. He is currently working as an Assistant Professor in the Department of Electrical Engineering at the Indian Institute of Science, Bangalore, India. His primary areas of interests are in power electronics and distributed generation, power quality, high power converters, and motor drives.